Acoustic Soft Tactile Skin (AST Skin)

Vishnu Rajendran S, Willow Mandil, Simon Parsons, and Amir Ghalamzan E*

Abstract-Acoustic Soft Tactile (AST) skin is a novel softflexible, low-cost sensor that can measure static normal forces and their contact location. This letter presents the design, fabrication, and experimental evaluation of AST skin. The proposed AST skin has some Acoustic channels(s) (ACs) arranged in parallel below the sensing surface. A reference acoustic wave from a speaker unit propagates through these ACs. The deformation of ACs under the contact force modulates the acoustic waves, and the change in modulation recorded by a microphone is used to measure the force magnitude and the location of the action. We used a static force calibration method to validate the performance of the AST skin. Our two best AST configurations are capable of (i) making more than 93% of their force measurements within \pm 1.5 N tolerances for a range of 0-30⁺¹ N and (ii) predicting contact locations with more than 96% accuracy. Furthermore, we conducted a robotic pushing experiment with the AST skin and an off-the-shelf Xela uSkin sensor, which showed that the AST skin outperformed the Xela sensor in measuring the interaction forces. With further developments, the proposed AST skin has the potential to be used for various robotic tasks such as object grasping and manipulation.

Index Terms—tactile sensing, soft-skin, acoustics, manipula-

I. INTRODUCTION

accurately measuring physical interactions is crucial for many physical robotic tasks, including human-robot interaction [1], object grasping, and manipulation [2]. Tactile sensing technologies have been developed and improved to enable robot agents to understand their environment better, leading to safer, more precise, and more efficient actions in a broader range of physical interaction tasks [3], [4], [5].

In the context of manipulation tasks, soft tactile sensors are gaining importance as a retrofit to end effectors after understanding the relevance of soft object handling. These sensors feature a soft, flexible sensing surface whose deformation provides tactile information such as force, contact location, and contact surface maps. Soft tactile sensors utilise both electronic (e.g., resistive [6], capacitive [7], piezoelectric [8], magnetic [9], [10], impedance [11]) and non-electronic transduction methods (e.g., camera-based [12], [13], [14], [15], [16], [17], [18], fluid-based [19], and acoustics [20], [21], [22], [23]) and their combinations [24] for converting the deformation to valuable tactile information.

Despite the progress in soft tactile sensing technology, several limitations persist: (i) many off-the-shelf soft tactile sen-

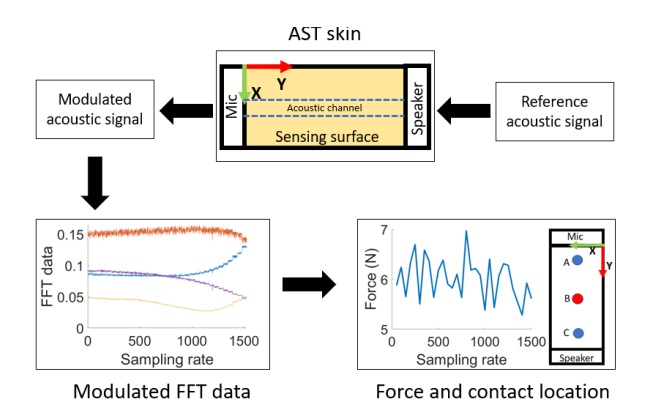


Fig. 1: AST Skin Overview: The force applied to the AST skin surface deforms the ACs beneath the sensing surface. These channels contain reference acoustic waves that travel from the speaker to the microphone. The acoustic wave amplitude is modulated in proportion to the deformation. We use FFT to transform the modulated waves to a frequency domain and ML methods to find the correlation between the force and its contact location, which resulted in the deformation.

sors come with a fixed topology and form factor, making integration/interfacing with existing hardware (eg:end-effectors) challenging, (ii) embedded electronics within the tactile sensor are vulnerable to cross-talk noise [25], (iii) requirement of making compact electronic sensory pick up behind sensing surface needs sophisticated manufacturing techniques, (iv) using camera-based transduction methods necessitate large amounts of space and their cumbersome structure makes integration into robotic end-effectors more challenging [14], [26], and (v) fluid-based transduction methods provide a delayed response to forces[25].

Among various acoustic-based soft tactile sensors, Zoller et al. [27] has developed a tactile sensing mechanism for a soft pneumatic finger with minimal hardware and complexities. The finger houses an internal speaker and microphone that continuously monitors changes in sound modulation due to finger deformation caused by external physical interactions, enabling the calculation of tactile information. This tactile sensing method allows the finger to measure contact forces, contact location, and the nature of material that comes in contact with it with a certain precision[28]. This sensing modality can be exploited to overcome some critical shortcomings of the soft tactile sensors presented above.

In this letter, we introduce Acoustic Soft Tactile skin (AST skin) technology (Fig. 1) inspired by a pneumatic finger with a sense of touch [29]. The AST skin is a silicone-based tactile skin with hollow passages that act as Acoustic Channels (ACs) and deform in response to external physical interactions. AC

This work was supported by Lincoln Agri-Robotics as part of the Expanding Excellence in England (E3) Programme

¹Lincoln Institute of Agri-Technology (LIAT) and Lincoln Centre of Autonomous Systems (LCAS), University of Lincoln, Lincoln, United Kingdom

²Lincoln Centre of Autonomous Systems (LCAS) and School of Computer Science, University of Lincoln, Lincoln, United Kingdom

^{*}Corresponding author

aghalamzanesfahani@lincoln.ac.uk

deformation modulates the continuous acoustic waves passing through them, which are processed using Fast Fourier Transform and Machine Learning (ML) techniques to estimate the contact force and its location. Unlike [27], [28], the AST skin can act as a standalone tactile sensing skin that can be attached to flat and non-flat surfaces. Moreover, they can be easily fabricated into any shape and size as long as it is possible to embed acoustic channels below the sensing surface. The AST skin design allows the speaker and microphone to be far away from the sensing surface, it makes it easy to attach the skin to existing hardware, e.g., end effectors with space constraints. The contributions of this research include presenting the novel AST skin technology, comparing various ML methods for force and contact position estimation, testing different AC topologies, and speaker-microphone configuration to optimise tactile sensing behaviour. We demonstrate the effectiveness and superiority of the AST skin through a comparison study with the off-the-shelf Xela uSkin tactile sensor.

II. RELATED WORKS

Acoustic methods have been used to measure tactile information, such as contact deformations, forces, and surface shape recognition. In this section, we explore research surrounding these tasks.

Measuring contact deformations: H. Shinoda et al. [30] created a silicone-based hemispherical fingertip that consists of an embedded ultrasound transmitter and receiver array. The fingertip measures deformations up to 10µm, and sensing surface inclination changes up to 0.001 radians. Building on this design, H. Shinoda et al. [21] introduced a hollow spherical cavity inside a flexible membrane. Equipped with an ultrasound transmitter and receiver, detecting the acoustic resonant frequency of the air inside to indicate the principal stress around the cavity. K. Teramoto et al. [23] proposed a flexible sensing membrane with acoustic transmitters and receivers on the substrate beneath, which can measure the curvature of objects encountering the membrane. Y. Tanaka et al. [22] developed an acoustics-based tactile sensor probe for real-time lump detection in laparoscopic surgery. The sensor probe is a silicone-based hollow tube. A speaker emits sound waves into the tube, and a microphone records the reflected waves from the end of the probe to detect wave deformation caused by contact with a lump.

Measuring force and other contact surface features: Chuang et al. [20] developed an ultrasonic tactile sensor that can measure normal static force in real-time (ranging from 1 to 6 N) and recognise shapes. The sensor uses ultrasonic sound pulses and measures variations in time of flight when the sensing when the elastomeric sensory surface undergoes deformation. The sensor includes a Thin Film Transistor layer between piezoelectric PVDF transmitter and receiver layers with a soft polymer sensing surface. In addition to measuring standard tactile information such as deformations, contact forces, and contact surface shapes, V. Wall et al. [28] demonstrated that active acoustic methods could be used to characterise force contact location and the material of contact objects by a soft pneumatic finger with a speaker and

microphone enclosed in the finger cavity. Also, the same pneumatic finger, when housing a single microphone alone (passive acoustic method), can measure contact forces, their location, and contact materials [29]. But this measuring capability is limited to situations when the contact results in some sound that propagates to the microphone.

These reports showcase the potential of using acoustic techniques to extract tactile information from soft material deformation. To simplify skin design, it is advisable not to integrate complex circuitry into the skin, as demonstrated by the tactile sensing utilised in pneumatic actuators [29], [28]. It is also beneficial to relocate the sensory hardware away from the sensing surface to ensure sensor compactness and avoid requiring sophisticated manufacturing techniques. This approach enables shaping the skin into various form factors, as dictated by the application. The sensor we developed in this letter maintains these strengths and can be easily calibrated and customized for various use cases.

III. ACOUSTIC SOFT TACTILE SKIN

Figure 1 provides an overview of AST Skin technology. The deformable membrane of the skin is served by a speaker unit and a microphone arranged on opposite sides. The speaker unit generates continuous acoustic waves that travel through the ACs, and the microphone receives the acoustic waves. As the channels deform due to external physical interactions, the amplitude of the acoustic waves changes (see Fig 6), and we leverage ML models to capture the relationship between the amplitude changes and the tactile information.

A. Design

To demonstrate this technology, we fabricated a flat, rectangular-shaped silicone skin measuring 35 mm x 60 mm. We investigate various configurations with single and dual ACs with simple geometrical shapes, such as cylindrical and conical, that run through the length of the skin. The diameter of the cylindrical AC is 5 mm, while the conical AC has diameters of 5 mm and 3 mm. The ACs connect the speaker-microphone arrangement of the skin. To ensure portability and ease of testing, we mount the skin inside a 3D-printed casing. However, we plan for skin designs without a hard case in our future work. The details of our prototype design and the different skin configurations tested are presented in the following sections.

a) Acoustic Channel Design: The impact of contact deformation on acoustic waves varies with the shape of the ACs, which we exploit to estimate force and contact location. We investigated the effect of different channel configurations on feature extraction for force and contact location (see Fig 2 for AC designs).

We studied single-channel and dual-channel configurations to verify our hypothesis that ACs can be used to predict tactile information. The study on single-channel skin configuration (AST 1) verifies the usability of this tactile skin, which calls for a narrow sensing region. For a broader sensing surface, the skin requires multiple channels, which we explore with studies on dual ACs (AST 2a-b, AST 3a-b, AST 4a-d) as an initial

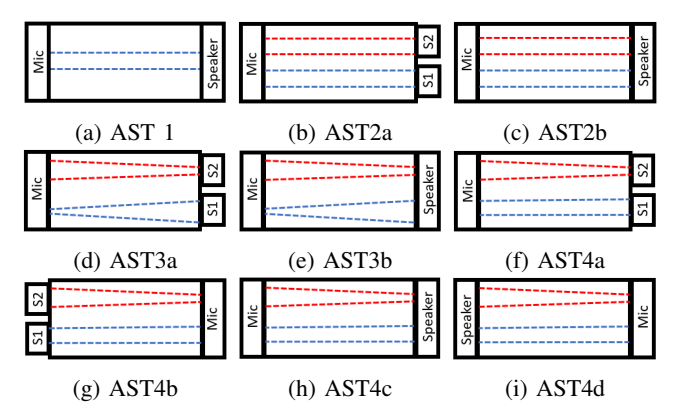


Fig. 2: AST skin configurations

step. In future works, we will explore using multiple channels with different geometries spanning the entire skin area.

For single-channel skin (AST 1), we considered a cylindrical-shaped channel. For dual channel skin configurations, we have used combinations of (1) two cylindrical-shaped channels (AST 2a, AST 2b), (2) two conical-shaped channels (AST 3a, AST 3b), and (3) a conical-shaped channel with cylindrical-shaped one (AST 4a-4d).

By providing these channel configurations, we tested two primary design parameters: (1) whether AC with a non-varying cross-section (cylinder) can distinguish forces acting on different points along their length? (2) for dual-channel skins, whether ACs with different geometrical shapes (AST 4a-4d) can best capture the tactile information compared to skins with similar AC geometries (AST 2a-2b, AST 3a-3b)?

We did not experiment with a single conical channel or a combination of two conical channels that are not inverted to each other. This is due to the assumption that the smaller diameter end of the channel will shut off earlier than the larger diameter end, resulting in a lower force measurement range. To mitigate this, we introduced conical-shaped channels which are inverted to each other (AST 3a, AST 3b).

b) Speaker Configurations: Speaker configurations are the second primary design feature we investigated in this work. We used a single speaker for AST 1, AST 2b, AST 3b, AST 4c, and AST 4d. For AST 2a, AST 3a, AST 4a-4b, we provided an individual speaker for each channel.

These speaker arrangements enable us to study the differences in skin performance (1) when all channels are provided with a single speaker versus each channel with an individual speaker and (2) when the speakers are arranged on the smaller and larger diameter ends of the conical channel (AST4a and 4b, AST4c and 4d). In this study, we used computer headphone speakers and a microphone, which will be replaced with a miniature type in further development studies.

B. Prototyping Process

The prototyping process employed in this work involves using cost-effective materials and a streamlined production process to enable the agile development of skin prototypes. The skin casing, as well as the speaker-microphone housings and channel inserts, are 3D printed using PLA material on

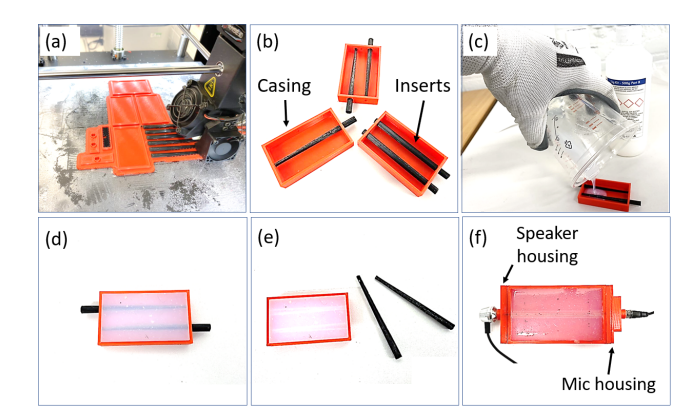


Fig. 3: Prototyping process: (a) 3D printing the sensor casing, inserts, and speaker-mic housings (b) Arranging the inserts into sensor casing (c) Pouring the silicon rubber into the casing (d) Curing (e) Removing inserts from the sensor casing (f) Mounting the speakers and mic

a Raisen Pro 3D printer. A Polycraft Silskin silicone rubber material, with a shore hardness value of A13 and a 1:1 catalyst ratio, is then poured into the 3D printed casing after positioning the channel inserts. After curing, the inserts are removed, leaving the desired channel cavities in the cured silicone rubber. Subsequently, the speaker(s) and microphone are mounted to their housing and then fastened to the casing following the configurations presented in Fig.2. The prototyping process is illustrated in Fig.3.

For the sake of simplicity, we will refer to the AST skin with the casing as AST skin in the subsequent sections of this letter.

C. Extracting Tactile Feature from Acoustic Signal

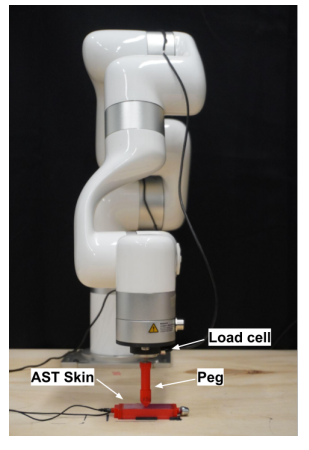
Here, we outline the methodology for generating two tactile features, the normal force (Newtons) and their contact location. We created a dataset using a robot arm and load cell by applying force to a series of locations on the soft skin. And these data are then processed and applied ML methods to predict the tactile features.

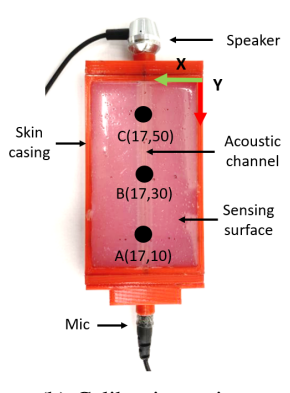
a) Sensor Calibration: The calibration setup consists of a 6 DOF robot arm¹ with a calibrated high-precision load cell mounted on the robot flange. This in-line load cell measures up to 1 KN of force, has an inbuilt driver board for USB communication with the PC, and is mounted with a wedge-shaped 3D-printed peg as shown in Fig. 4a.

Here we used a robotic arm to apply a known force through the load cell and peg on specific locations on the AST skin. We initially considered three calibration points on the skin surface for all configurations, namely A(17,10), B(17,30), and C(17,50), as illustrated in Fig. 4b. These points are crucial, as point A is closer to the mic, point C is closer to the speaker, and point B is between the mic and speaker(s).

Before the calibration process, we placed the AST skin in a fixed position over the workbench, as shown in Fig.4a, and played a continuous reference acoustic signal through the

¹The UFactory xArm by ufactory.cc





(a) Robot based calibration setup

(b) Calibration points

Fig. 4: AST skin calibration

speaker(s). The details of this reference signal are provided in the forthcoming subsection. The robot arm is then driven to each calibration point one by one, and on each point, the peg pushes by the arm with an increment of 0.2 mm. As the central axis of the peg passes vertically through the designated points, the AC(s) are compressed uniformly. At each incremental step of 0.2 mm, the corresponding load cell readings are recorded, and simultaneously, the mic recorded 50 samples of the sound signal it received. This process continued until the load cell reading reached 30⁺¹ N. In our future studies, we will calibrate these skins for multiple calibration points spanning the whole length and width of the skin design with different contact shapes.

- b) Reference Acoustic Signal: A test reference acoustic signal is generated using Audacity. It comprises four sine waves of frequencies of 300 Hz, 500 Hz, 700 Hz, and 900 Hz and with individual amplitudes of 0.6 (on a 0 to 1 scale). During the sensor operation, this reference signal is played through the speaker(s).
- c) Data Processing: The data processing pipeline used in the calibration process is shown in Fig. 5. For each AST skin configuration, the resulting dataset after data processing contains the load cell reading with the corresponding location of loading (A, B, or C) and the amplitudes of the selected frequencies of the sound signal. Fast Fourier Transform (FFT) algorithm determines the amplitudes of the acoustic signals received by the microphone (FFT data). For each skin model, a total of 5100 data points are generated, with 1700 data points each for the three locations, A, B, and C.
- d) Force and Contact Location Estimation: Our analysis revealed that the amplitudes of individual frequency components in the reference signal (FFT data) vary with an increase in force from 0 to 30⁺¹ N at each location A, B, and C on the AST skin. Fig. 6 presents a sample of these variations for AST 1. Based on this finding, we confirm that the FFT data can be used to predict unknown forces and their contact locations. Therefore, we express the unknown force and its location as:

$$(F_i, L_i) = f(A_{300i}, A_{500i}, A_{700i}, A_{900i})$$
(1)

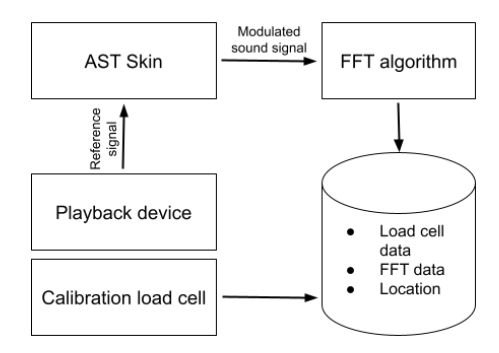


Fig. 5: Data processing pipeline

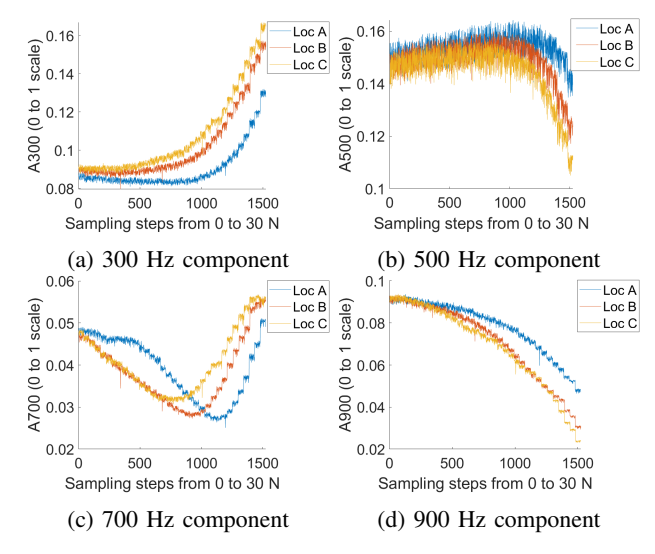


Fig. 6: Variation of FFT data at locations A, B, and C when force varies from 0 to 30^{+1} N

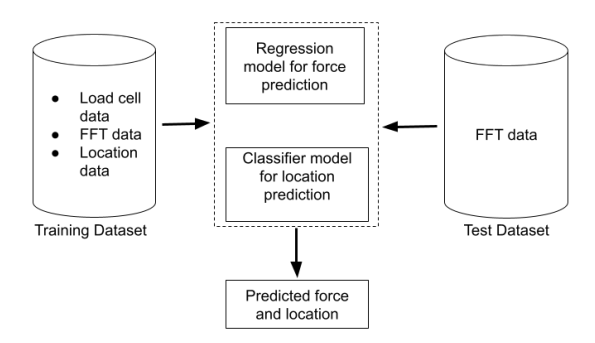


Fig. 7: Schematic of the ML model for contact force and location estimation

where F_i is the unknown force at instance i, $A_{300i}, A_{500i}, A_{700i}, A_{900i}$ are the amplitudes of frequency components 300 Hz, 500 Hz, 700 Hz, and 900 Hz recorded at the same instance (FFT data), and L_i is the location of contact (A, B or C).

We used a regression and classifier ML model to predict the unknown force and contact location from the FFT data, respectively, as illustrated in Fig.7. The selection of the optimum model is made through a comparative study presented in the following section.

IV. RESULTS AND DISCUSSIONS

We have done a systematic study to find the best configurations of ACs, speaker-microphone, and optimal ML models for tactile feature extraction. So this section answers the following key questions: (1) What is the impact of ACs and speaker configurations on force and contact location prediction? (2) Which ML model is selected to develop the prediction model for each AST skin? (3) What is the performance of force and contact location prediction? (4) Can the AST Skin measure static push force during an object-pushing test case, and how does it perform against a state-of-the-art Xela uSkin tactile sensor?

Performance Metrics: The following metrics present the outcomes of the tests conducted to present the findings. (1) We use the validation error/efficiency obtained for the dataset corresponding to each AST skin for selecting the regression and classifier model. (2) The force prediction performance of each AST skin is presented as the percentage of predictions that fall within ± 0.50 N, ± 1 N, and ± 1.50 N tolerance of the actual force values. (3) The contact location prediction performance is presented as the total number of true predictions per test (each skin location is tested for 170 trials), and they are averaged to define the overall accuracy. (4) For the object-pushing test case, we compare the force-measuring performance of the AST skin and the Xela sensor in terms of their absolute error in the measured force.

A. Selection of Machine Learning Model

We compared various regression and classifier models based on their validation errors/accuracy for each AST skin data. The models are trained using a dataset partition of 90:10 and 10-fold cross-validation. The regression model with the minimum validation error and the classifier with the maximum accuracy is selected for predicting force and location, respectively. The comparison results are presented in tables I and II, and the selected models for each AST skin are highlighted in the tables. The details of force and location predictions using these models are presented below.

B. Force Prediction

The force prediction performance of the AST skins is presented in Fig. 8, showing the percentage of force predictions falling within ± 0.5 N, ± 1 N, and ± 1.5 N tolerances. The performance of each skin configuration is analysed with respect to the effect of speaker configuration and AC geometries.

a) Effect of Speaker Configuration: The presented results in Fig 8 indicate that the dual-channel skin configurations with a single speaker (AST2b, AST3b, AST4c, AST4d) mostly outperformed or showed comparable performance to their individual speaker designs (AST2a, AST3a, AST4a, AST4b). This suggests that a single speaker can serve multiple channels without compromising performance. This finding implies that the skin technology is potentially scalable, and a skin with multiple channels may not require an equal number of speakers. However, further investigation is needed to confirm this claim. We also tested the effect of positioning speakers on different ends of channels, but the results did not show any significant impact on the sensor performance.

b) Effect of Acoustic Channel Geometry: The single-channel AST1 configuration demonstrated a force prediction accuracy of 82.74% within ± 0.5 N tolerance range and 93.5% within ± 1 N range, indicating that a single channel with a uniform geometrical shape can accurately infer contact forces acting on different points. Other skin configurations were also tested to investigate the feasibility of using an array of AC to serve a skin that may require a broader sensing surface area. The results in Fig. 8 show that considerably better performance can be achieved when the channel geometries are non-identical and a single speaker unit serves all channels. This is evident when comparing the performance of skin configuration AST3b, AST4c, and AST4d with AST2b.

C. Contact Location Prediction

Table III presents the accuracy of each AST skin configuration for predicting the contact locations. All skin configurations achieved a high prediction accuracy of more than 89%. The results indicate that the location prediction performance is improved when a single speaker serves the AC(s). Apart from this, no other significant factors were found that greatly influenced the location prediction capability of the skin.

After analysing the results of force and location predictions and their underlying factors, several conclusions can be drawn: (1) A smaller-width skin can utilise a single acoustic channel to measure contact force and its location accurately. Furthermore, the channel can have a simple geometry, such as a cylinder. Even though it has a uniform shape along its length, it can still distinguish forces and their locations applied at different points, (2) For skin with a broader sensing surface area, an array of ACs can be used, and individual speakers for each channel may not be necessary (3) The use of different geometrical shapes for each AC may lead to the improved performance of the skin.

D. Pushing Experiment with AST and Xela uSkin Sensor

We conducted a static pushing experiment to evaluate the performance of our preliminary design of the acoustic tactile (AST) sensor. The test involves pushing a fixed box on the worktable (Fig 9) with the AST skin mounted to an extension attached to the flange of uFactory arm. Also, we performed the same pushing experiment using the Xela uSkin sensor² for performance comparison. Xela sensor has a 4 x 4 array of sensing units called taxels which act as force-pickup units.

For this experiment, we selected AST 1 from the various AST skins presented, as it provided better accuracy in predicting the forces during calibration. We recalibrated the skin before the experiment to avoid variation in measurement quality due to any unseen factors. The box used in this experiment was provided with a load cell to understand the interaction force and compare it with the force value measured by the sensors. The load cell is mounted with the same wedge-shaped peg used during the AST cell calibration. Three static normal forces (6 N, 12 N, and 18 N) are applied to the box through the load cell by driving the robot arm. This force range

²The uSkin sensor by xelarobotics.com

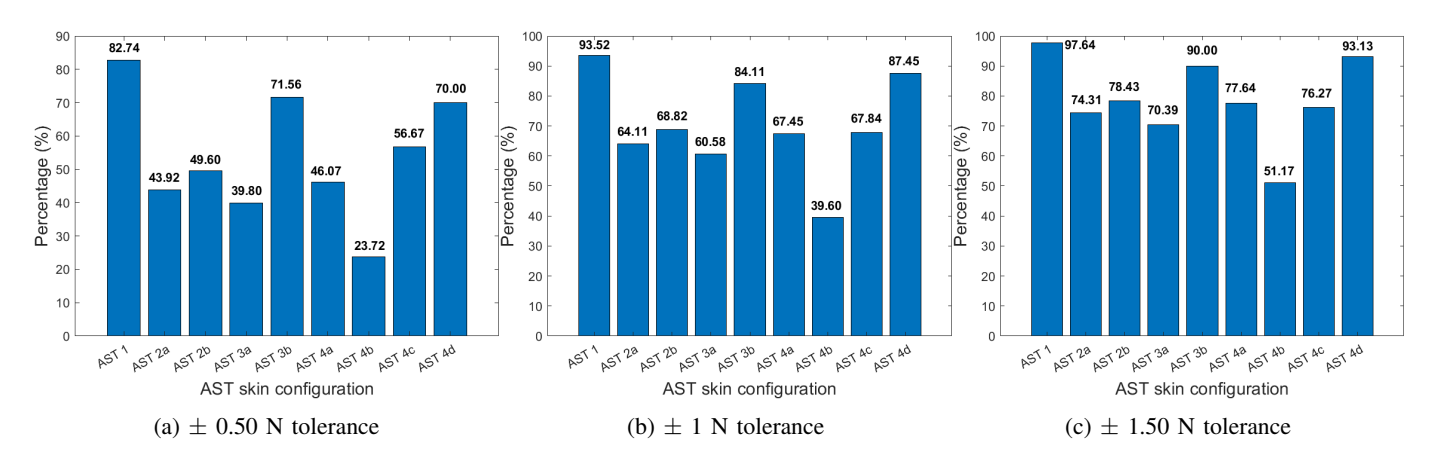


Fig. 8: Percentage of force predicted with \pm 0.50 N, \pm 1 N, and \pm 1.50 N tolerance

TABLE I: Comparison of various regression models based on validation error for predicting contact force

Regression models	AST skin configuration									
Regression models	AST 1	AST 2a	AST 2b	AST 3a	AST 3b	AST 4a	AST 4b	AST 4c	AST 4d	
Linear Regression										
Linear	2.22	5.98	7.23	4.87	2.85	7.28	7.17	5.91	3.66	
Interactions Linear	1.78	5.01	6.45	3.45	2.04	6.61	6.102	5.54	3.13	
Robust	2.54	6.33	7.74	6.13	3.81	9.17	8.29	6.72	3.66	
Stepwise Linear	1.78	5.01	6.46	3.46	2.04	6.61	6.11	5.54	3.14	
Regression Trees										
Fine Tree	1.08	3.19	4.34	2.82	1.31	4.07	4.69	3.27	1.59	
Medium Tree	1.18	3.02	4.26	2.62	1.24	3.86	4.5	3.1	1.625	
Coarse Tree	1.42	3.5	4.52	2.58	1.31	4.2	4.73	3.49	1.73	
Support Vector Machines										
Linear	2.4	6.1	7.52	5.39	2.94	8.09	7.41	6.18	3.74	
Quadratic	1.93	5.98	6.96	3.62	2.09	7.98	5.82	5.63	2.95	
Cubic	2.29	28.81	12.43	21.54	10.02	17.45	28.25	15.23	24.8	
Fine Gaussian	1.04	2.42	4.34	2.319	1.3	3.31	3.7	2.95	1.33	
Medium Gaussian	1.24	3.29	4.26	2.73	1.52	3.96	4.5	3.98	1.77	
Coarse Gaussian	1.67	4.68	4.52	3.22	2	5.92	5.68	5.45	2.78	
Gaussian Process										
Rational Quadratic	0.72	2.21	3.4	2.16	1.08	3.34	3.59	2.56	1.22	
Squared Exponential	0.87	2.41	3.31	2.25	1.17	3.27	3.65	2.72	1.26	
Matern 5/2	0.8	2.27	3.24	2.2	1.14	3.29	3.6	2.61	1.2	
Exponential	0.72	2.24	3.35	2.15	1.06	3.25	3.6	2.53	1.18	
Ensemble of Trees										
Boosted Trees	1.67	3.6	4.6	2.57	1.56	3.88	4.59	3.65	1.8	
Bagged Trees	0.94	2.63	3.67	2.29	1.08	3.41	3.86	2.62	1.3	
Neural Networks										
Narrow Neural Network	1.2	3.48	5.21	2.83	1.47	4.63	4.8	3.86	1.62	
Medium Neural Network	1.15	2.88	4.94	2.53	1.49	3.74	4.27	3.305	1.51	
Wide Neural Network	1.05	2.89	4.32	2.35	1.37	3.64	3.85	2.89	1.34	
Bilayered Neural Network	1.07	2.68	5.27	2.36	1.29	3.63	4.33	5.13	1.41	
Trilayered Neural Network	0.9	2.52	4.03	2.28	1.29	3.42	3.95	2.94	1.31	

is selected as the measuring range of Xela uSkin is 0 to 18 N. We conducted 30 pushes on the box with above mentioned normal static loads with contact making at the middle of the sensory surface of both sensors (location B for AST skin). The absolute error in force measured by both sensors is presented in Fig 10.

The results showed that the AST skin could predict the normal forces of 6 N, 12 N, and 18 N with a mean error of -0.01 N, 0.01 N, and -0.44 N, respectively, while the Xela sensor predicted them with a mean error of 2.03 N, 2.51 N, and 0.89 N, respectively.

In this pushing experiment, the Xela sensor showed a relatively higher error, possibly because the loading contact might not be exactly acted on the taxels. In contrast, the AST skin showed better performance in this loading situation

because it does not rely on individual force-pickup units but rather on channel deformation to predict force.

Our study demonstrates the potential of AST skin technology to be used in real-time static normal force-measuring applications, as it showed comparable performance to an off-the-shelf soft tactile sensor.

Overall, the AST skin has the potential to become a valuable tool for tactile measurements. Our future work on the AST skin will include calibrating the sensor for dynamic normal and shear force measurement with continuous 2D sensing points on the skin surface. Moreover, AST skin technology will be tested for real-time applications, such as robotic manipulation, human-robot interaction, and medical diagnosis.

TABLE II: Comparison of various classifier models based on validation accuracy for predicting contact force locations

Cl. 'C M 11	AST skin configuration								
Classifier Models	AST 1	AST 2a	AST 2b	AST 3a	AST 3b	AST 4a	AST 4b	AST 4c	AST 4d
Tree									
Fine Tree	91.3	93.2	95	90.5	86.1	89.8	92.7	95.6	93.9
Medium Tree	78.8	92.9	85.8	87.6	74.2	85.7	90.1	94.8	78.5
Coarse Tree	69.9	87.1	71	74.5	60.2	77.1	84.2	87.6	67
Discriminant Analysis									
Linear Discriminant	70.7	89.4	89.2	74.8	59	79	82.1	70.4	73.5
Quadratic Discriminant	70.3	89	89.5	79	58.4	80.6	88	88	87.3
Naïve Bayes Classifiers									
Guassian Naïve Bayes	42.2	73.9	72.7	46.3	39.2	74	79.2	63.8	60.9
Kernal Naïve Bayes	72.6	84.2	78.1	77.2	61.9	77.3	86.6	89.7	73.9
Support Vector Machines									
Linear	77.2	92.4	88.5	78.4	62.7	84.4	86	83.4	84.4
Quadratic	94.3	91.9	93.5	90.2	61.1	88	93.6	96.1	89.1
Cubic	72	65.9	95.7	48.2	53.2	64.5	60.8	71.8	74.9
Fine Guassian	96	95.7	98.1	92.2	87.8	92.6	95.4	97.2	97.1
Medium Guassian	94.4	94.1	93	91.3	81.3	91.2	93.8	95.9	93.2
Coarse Guassian	74.4	91.8	88.7	88.5	63.9	85.6	89.1	86.8	87.5
Nearest Neighbor Classifier									
Fine KNN	95	94.5	97.7	90.2	89.3	91.2	93.7	96.6	96.6
Medium KNN	94.9	95.4	98	92.1	91	92.7	94.7	97	97.3
Coarse KNN	82.7	93.4	93.4	89.8	81	91.1	93.2	93.6	92.7
Cosine KNN	86.6	93.7	95.5	90	85.3	89.4	92.6	89.2	90.7
Cubic KNN	94.4	95.3	98	91.8	90.6	92.7	94.7	97	97.2
Weighted KNN	95.8	95.6	98.2	92.1	91	92.8	94.8	97.2	97.3
Ensemble Classifiers									
Boosted Trees	82.7	94.1	94.1	90.4	75.8	89.8	92.7	96	91.1
Bagged Trees	96.4	95.4	97.6	91.8	91.9	92.6	94.7	96.9	96.8
Subspace Discriminant	50.9	78.4	85.3	60.8	49.7	75.4	84.1	66.9	74.1
Subspace KNN	89.7	91.8	90	84.1	82.1	85.4	86	92.7	91.4
RUSBossted Trees	78.8	92.4	85.8	87.6	74.2	85.7	90.1	94.9	78.5
Neural Network Classifiers									
Narrow Neural Network	95.6	92.4	96.9	91.7	86.7	92.2	94.7	96.9	95.8
Medium Neural Network	96.3	94.7	97.8	92.3	89.4	92.5	95.3	97.1	97.2
Wide Neural Network	96.1	94.9	97.6	92.2	90.3	92.5	94	97	96.8
Bilayered Neural Network	96.2	94.9	97.2	92.5	89	91.8	94.9	96.9	96.9
Trilayered Neural Network	95.8	95.1	97.6	92.4	89.3	92.4	94.5	97.2	97

TABLE III: Predicted location of contact force

AST skin	True	predic	Accuracy		
configuration	A	В	С	(%)	
AST 1	169	160	164	96.66	
AST2a	169	168	153	96.07	
AST2b	168	169	168	99.01	
AST3a	165	150	161	93.33	
AST3b	163	142	150	89.21	
AST4a	168	151	155	92.94	
AST4b	168	156	162	95.29	
AST4c	168	165	166	97.84	
AST4d	168	167	162	97.45	

V. CONCLUSIONS

We have presented the design, fabrication, and testing of a novel Acoustic Soft Tactile skin (AST skin). The AST skin uses Acoustic Channels beneath the sensing surface to measure the contact normal force and its location based on the principle of the wave modulation. To validate the concept, we have prototyped and studied nine AST skins with different configurations of Acoustic Channels and acoustic hardware (speaker-mic). During our study, two AST skin designs made more than 93% of static normal force predictions with ± 1.5 N tolerance for a full-scale force range of 0-30⁺¹ N. Also, they made more than 96% accurate force contact location predictions. We have also demonstrated the superiority and

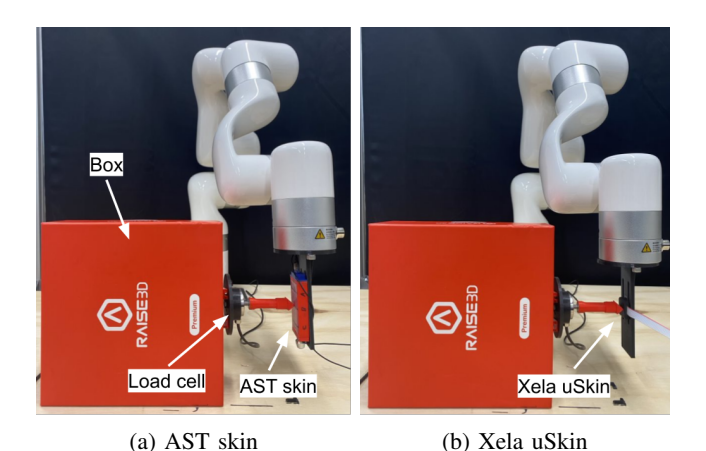


Fig. 9: Pushing experiment with AST skin and Xela sensor

effectiveness of the AST skin in measuring static normal forces in a pushing experiment against an off-the-shelf soft tactile sensor (Xela uSkin).

REFERENCES

 M. Fritzsche, N. Elkmann, and E. Schulenburg, "Tactile sensing: A key technology for safe physical human robot interaction," in *Proceedings* of the 6th International Conference on Human-robot Interaction, 2011, pp. 139–140.

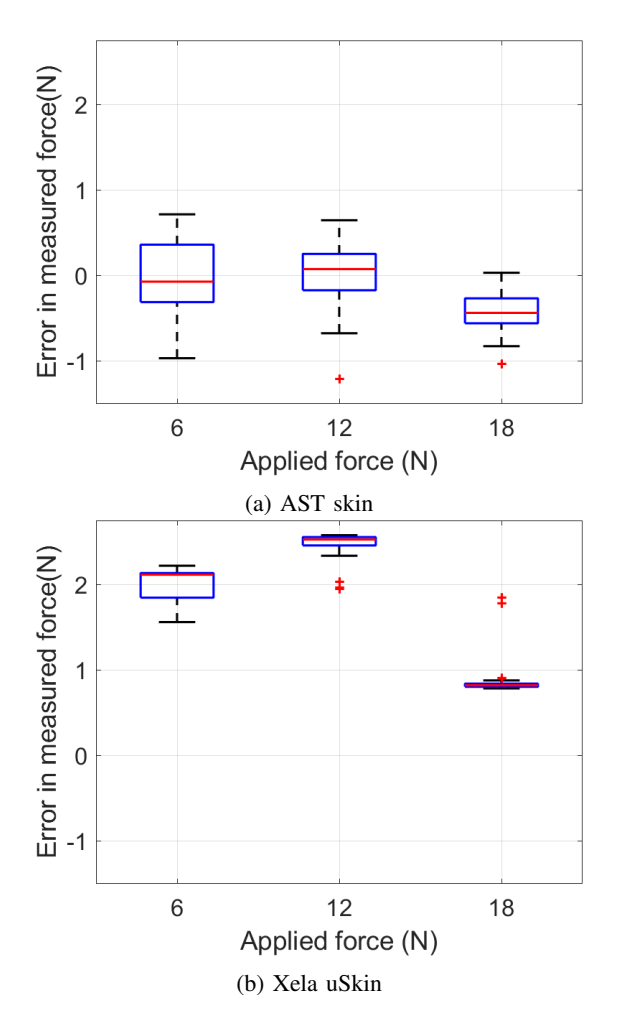


Fig. 10: Absolute error in the force measured by AST skin and Xela sensor during the pushing experiment

- [2] H. Yousef, M. Boukallel, and K. Althoefer, "Tactile sensing for dexterous in-hand manipulation in robotics—a review," *Sensors and Actuators A: physical*, vol. 167, no. 2, pp. 171–187, 2011.
- [3] W. Mandil, K. Nazari, and A. Ghalamzan, "Action Conditioned Tactile Prediction: case study on slip prediction," in *Proceedings of Robotics: Science and Systems*, New York City, NY, USA, 6 2022.
- [4] R. S. Dahiya, G. Metta, M. Valle, and G. Sandini, "Tactile sensing—from humans to humanoids," *IEEE transactions on robotics*, vol. 26, no. 1, pp. 1–20, 2009.
- [5] J. Dargahi and S. Najarian, "Advances in tactile sensors design/manufacturing and its impact on robotics applications—a review," *Industrial Robot: An International Journal*, 2005.
- [6] J. Zimmer, T. Hellebrekers, T. Asfour, C. Majidi, and O. Kroemer, "Predicting grasp success with a soft sensing skin and shape-memory actuated gripper," in 2019 IEEE/RSJ International Conference on Intelligent Robots and Systems (IROS). IEEE, 2019, pp. 7120–7127.
- [7] Q. Li, Z. Ullah, W. Li, Y. Guo, J. Xu, R. Wang, Q. Zeng, M. Chen, C. Liu, and L. Liu, "Wide-range strain sensors based on highly transparent and supremely stretchable graphene/ag-nanowires hybrid structures," *Small*, vol. 12, no. 36, pp. 5058–5065, 2016.
- [8] K. Song, S. H. Kim, S. Jin, S. Kim, S. Lee, J.-S. Kim, J.-M. Park, and Y. Cha, "Pneumatic actuator and flexible piezoelectric sensor for soft virtual reality glove system," *Scientific reports*, vol. 9, no. 1, p. 8988, 2019.
- [9] M. Rehan, M. M. Saleem, M. I. Tiwana, R. I. Shakoor, and R. Cheung, "A soft multi-axis high force range magnetic tactile sensor for force feedback in robotic surgical systems," *Sensors*, vol. 22, no. 9, p. 3500, 2022.
- [10] G. Diguet, J. Froemel, M. Muroyama, and K. Ohtaka, "Tactile sensing using magnetic foam," *Polymers*, vol. 14, no. 4, p. 834, 2022.

- [11] H. Wu, B. Zheng, H. Wang, and J. Ye, "New flexible tactile sensor based on electrical impedance tomography," *Micromachines*, vol. 13, no. 2, p. 185, 2022.
- [12] B. Ward-Cherrier, N. Pestell, L. Cramphorn, B. Winstone, M. E. Giannaccini, J. Rossiter, and N. F. Lepora, "The tactip family: Soft optical tactile sensors with 3d-printed biomimetic morphologies," *Soft robotics*, vol. 5, no. 2, pp. 216–227, 2018.
- [13] D. F. Gomes and S. Luo, "Geltip tactile sensor for dexterous manipulation in clutter," in *Tactile Sensing, Skill Learning, and Robotic Dexterous Manipulation*. Elsevier, 2022, pp. 3–21.
- [14] W. Yuan, S. Dong, and E. H. Adelson, "Gelsight: High-resolution robot tactile sensors for estimating geometry and force," *Sensors*, vol. 17, no. 12, p. 2762, 2017.
- [15] E. Donlon, S. Dong, M. Liu, J. Li, E. Adelson, and A. Rodriguez, "Gelslim: A high-resolution, compact, robust, and calibrated tactilesensing finger," in 2018 IEEE/RSJ International Conference on Intelligent Robots and Systems (IROS). IEEE, 2018, pp. 1927–1934.
- [16] M. Lambeta, P.-W. Chou, S. Tian, B. Yang, B. Maloon, V. R. Most, D. Stroud, R. Santos, A. Byagowi, G. Kammerer et al., "Digit: A novel design for a low-cost compact high-resolution tactile sensor with application to in-hand manipulation," *IEEE Robotics and Automation Letters*, vol. 5, no. 3, pp. 3838–3845, 2020.
- [17] Z. Chen, S. Zhang, S. Luo, F. Sun, and B. Fang, "Tacchi: A pluggable and low computational cost elastomer deformation simulator for optical tactile sensors," *IEEE Robotics and Automation Letters*, vol. 8, no. 3, pp. 1239–1246, 2023.
- [18] C. Sferrazza and R. D'Andrea, "Design, motivation and evaluation of a full-resolution optical tactile sensor," *Sensors*, vol. 19, no. 4, p. 928, 2019.
- [19] D. Gong, R. He, J. Yu, and G. Zuo, "A pneumatic tactile sensor for co-operative robots," *Sensors*, vol. 17, no. 11, p. 2592, 2017.
- [20] C.-H. Chuang, H.-K. Weng, J.-W. Chen, and M. O. Shaikh, "Ultrasonic tactile sensor integrated with tft array for force feedback and shape recognition," *Sensors and Actuators A: Physical*, vol. 271, pp. 348–355, 2018.
- [21] H. Shinoda, K. Matsumoto, and S. Ando, "Acoustic resonant tensor cell for tactile sensing," in *Proceedings of International conference on Robotics and Automation*, vol. 4. IEEE, 1997, pp. 3087–3092.
- [22] Y. Tanaka, T. Fukuda, M. Fujiwara, and A. Sano, "Tactile sensor using acoustic reflection for lump detection in laparoscopic surgery," *Interna*tional journal of computer assisted radiology and surgery, vol. 10, pp. 183–193, 2015.
- [23] K. Teramoto and K. Watanabe, "Acoustical tactile sensor utilizing multiple reflections for principal curvature measurement," in SICE 2001. Proceedings of the 40th SICE Annual Conference. International Session Papers (IEEE Cat. No. 01TH8603). IEEE, 2001, pp. 339–344.
- [24] K. Park, H. Yuk, M. Yang, J. Cho, H. Lee, and J. Kim, "A biomimetic elastomeric robot skin using electrical impedance and acoustic tomography for tactile sensing," *Science Robotics*, vol. 7, no. 67, p. eabm7187, 2022
- [25] E. Fujiwara and L. de Oliveira Rosa, "Agar-based soft tactile transducer with embedded optical fiber specklegram sensor," *Results in Optics*, vol. 10, p. 100345, 2023.
- [26] N. F. Lepora, "Soft biomimetic optical tactile sensing with the tactip: A review," *IEEE Sensors Journal*, vol. 21, no. 19, pp. 21131–21143, 2021
- [27] G. Zöller, V. Wall, and O. Brock, "Active acoustic contact sensing for soft pneumatic actuators," in 2020 IEEE International Conference on Robotics and Automation (ICRA). IEEE, 2020, pp. 7966–7972.
- [28] V. Wall, G. Zöller, and O. Brock, "Passive and active acoustic sensing for soft pneumatic actuators," arXiv preprint arXiv:2208.10299, 2022.
- [29] G. Zöller, V. Wall, and O. Brock, "Acoustic sensing for soft pneumatic actuators," in 2018 IEEE/RSJ International Conference on Intelligent Robots and Systems (IROS). IEEE, 2018, pp. 6986–6991.
- [30] H. Shinoda and S. Ando, "A tactile sensor with 5-d deformation sensing element," in *Proceedings of IEEE International Conference on Robotics* and Automation, vol. 1. IEEE, 1996, pp. 7–12.